Geotech Geol Eng (2016) 34:1–14
DOI 10.1007/s10706-015-9923-3

ORIGINAL PAPER

Study on the Reasonable Height of Embankment in Qinghai–Tibet Highway

Songhe Wang · Jilin Qi · Fengyin Liu

Received: 23 June 2015 / Accepted: 1 September 2015 / Published online: 5 September 2015

Abstract A reasonable height of embankment is beneficial for maintaining the thermal and mechanical stability of highway in cold regions. This paper firstly introduced theoretical models for two main sources of settlement, including an improved consolidation theory for thawing permafrost and a simple rheological element based creep model for warm frozen soils. A modified numerical method for living calculating thaw consolidation and creep in corresponding domains and for post-processing the proportion of each source in total settlement based on the effective thaw consolidation time. Two typical geological sections underlain by warm permafrost layer were selected from the Qinghai–Tibet highway. The heat transfer and continuing settlement for two sections were modeled by assuming that the height of embankment ranges from 0 to 6.0 m. The reasonable critical height for two sections are 1.63 and 1.35 m, respectively, by comparing maximum thawing depth, mean annual temperature and settlement in the roadbed center. For two sections with design height of embankment, the proportions of thaw consolidation and creep to the total settlement were analyzed. For sections at higher ground temperature, thaw consolidation accounts for a major part while thaw consolidation of section L is a little larger than that of creep.

Keywords Cold regions · Thaw consolidation · Creep · Critical height · Effective thaw consolidation time

S. Wang (✉) · F. Liu
Institute of Geotechnical Engineering, Xi'an University of Technology, Xi'an 710048, Shaanxi, China
e-mail: wangsonghe@xaut.edu.cn

J. Qi
College of Civil and Transportation Engineering, Beijing University of Civil Engineering and Architecture, Beijing 100044, China

1 Introduction

Many large-scale highway engineering constructed in cold regions in China such as Qinghai–Tibet highway and Beijing–Lhasa national highway have played a significant role in promoting the regional economic development. As for the sections passing through permafrost areas, many engineering problems are arising under the dual effect of global warming and engineering activities (Andersland and Ladanyi 1994; Epps 2000; Lai and Zhang 2003; Ma et al. 2011), such as frost boiling, thaw slumping of slopes and cracks in pavements, settlement of embankments. These engineering problems significantly affect the service life of highway engineering; of which, the continuing settlement of embankments is a primary source (Qi et al. 2007; Wang et al. 2013).

The stability and durability of highway engineering in cold regions is closely related to the thermal state of permafrost, especially when asphalt pavement is involved. The asphalt pavement is made of both

construction aggregate and asphalt, which is a typical low-permeability material. It will enhance the absorption rate of solar radiation by 20 % and obviously hinder the migration of water underneath the roadbed, which further affects the heat transfer between atmosphere and asphalt pavement (Wu et al. 2001, 2002). The asphalt pavement results in two kinds of responses in permafrost layer to heat accumulation (Heike and Peter 2000; Thomas and Kevin 2003; Lai et al. 2009), i.e., (1) thawing of underlying permafrost and descending permafrost table; (2) continuing temperature rising in permafrost layer. The former leads to thaw consolidation, which has always been regarded as the primary source of settlement. It was firstly estimated by an empirical index, thaw settlement coefficient. Then a 1D consolidation theory for thawing soils was derived by Morgenstern and Nixon (1971). Yao et al. (2012) extended the theory into 3D and large strain conditions. Wang and Liu (2015) further improve the stress–strain behavior of thawing soils by a modified hypoplastic model. As for the latter case, creep of frozen soils will significantly increase when temperature rises (Qi et al. 2007). Ladanyi (1972) suggest an engineering creep model for frozen soils. Vyalov (1986) put forward creep equations for estimating creep deformation in foundations. Wang et al. (2014) proposed a simple rheological element based creep model for frozen soils and a case study shows that creep accounts for a significant part when warm and ice-rich permafrost is concerned.

The monitored data in Qinghai–Tibet highway shows that at a relatively low embankment the permafrost table develops downward while it tends to grow upward at higher embankments. A critical height of embankment is defined as the critical height at which the permafrost table stabilizes and the deformation mainly results from the compression of seasonal active layer. Thus a basic rule in designing a highway embankment is to maintain a stable permafrost table (Yu and Wu 1986). Wu et al. (1998) based on this principle analyzed the effect of height of fill, air temperature and active layer on the critical height. However, in some cases when asphalt pavements were used, the permafrost table descended, even when the embankment was heightened (Tong and Wu 1996).

This paper aims to propose a modified numerical method for live calculating thaw consolidation and creep in corresponding domains and for live determining the proportion of each source to the total settlement. Based on a comprehensive analysis of thermal regime and settlement, the reasonable height of embankment for two typical sections along Qinghai–Tibet highway will be discussed.

2 Models for Thaw Consolidation and Creep

2.1 Heat Transfer Equation

A reliable prediction of thermal regime is urgently needed to further analyze the stability and durability of cold regions engineering, especially to locate the thawing boundary in frozen ground, above which thaw consolidation occurred while creep of warm frozen soils initiated underneath. Taking into account the ice-water phase change, the heat transfer in frozen ground under complex atmospheric effect and engineering activities is quite a strongly nonlinear problem. For convenience of research, heat convection and radiation are not considered and only a heat conductive law considering ice-water phase change is given as follows

$$\begin{cases} -h_{i/i} + h_v = \rho C \dfrac{\partial T}{\partial t} \\ h_i = -\lambda T_{/i} \end{cases} \tag{1}$$

where h_v is the volumetric heat source intensity; h_{i} is the heat flux vector; ρ is the density of soil; C and λ are the equivalent specific heat and thermal conductivity, which can be determined by the following equations

$$C = \begin{cases} C_u & (T > T_p) \\ C_f + \dfrac{C_u - C_f}{T_p - T_b}(T - T_b) + \dfrac{L}{1+W}\dfrac{\delta W_i}{\delta T} & (T_b \le T \le T_p) \\ C_f & (T \le T_b) \end{cases} \tag{2}$$

$$\lambda = \begin{cases} \lambda_u & (T > T_p) \\ \lambda_f + \dfrac{\lambda_u - \lambda_f}{T_p - T_b}(T - T_b) & (T_b \le T \le T_p) \\ \lambda_f & (T \le T_b) \end{cases} \tag{3}$$

where C_{u} and C_{f} are the specific heat for post-thawed and frozen soil, respectively; λ_{u} and λ_{f} are the heat conductivity for post-thawed and frozen soil, respectively; L is the latent heat during ice-water phase change; W and W_{i} are the water and ice content; T_{p} and T_{b} are the upper and lower temperature limits of ice-water phase change.

2.2 Large Strain Consolidation Theory for Thawing Soils

Following the work by Qi et al. (2012), the kinematic variables based on the large strain description taking the current configuration as the reference coordinates were employed here and the governing equations for the mechanical behaviors of soil skeleton are given as

$$\sigma_{ij/j} + \rho g_i = \rho \frac{dv_i}{dt} \tag{4}$$

$$\dot{\varepsilon}_{ij} = \left(\frac{\partial v_i}{\partial x_j} + \frac{\partial v_j}{\partial x_i}\right) \Big/ 2, \quad \dot{w}_{ij} = \left(\frac{\partial v_j}{\partial x_i} - \frac{\partial v_i}{\partial x_j}\right) \Big/ 2 \tag{5}$$

$$\overset{\vee}{\sigma}_{ij} = \frac{d\sigma_{ij}}{dt} - \sigma_{ik}\omega_{ki} - \sigma_{jk}\,\omega_{kj} \tag{6}$$

$$d\overset{\vee}{\sigma}_{ij} = D^{ep}_{ijkl} d\varepsilon_{kl} \tag{7}$$

where $\dot{\varepsilon}_{ij}$ and $\dot{w}_{ij}$ are the symmetric strain rate tensor and skew-symmetric spin tensor, respectively; v_{i} (i = 1, 2 and 3) is the instantaneous velocity of the material point; $\overset{\vee}{\sigma}_{ij}$ is the Jaumann stress rate which eliminates the effect of rigid rotation; D^{ep}_{ijkl} is the elastoplastic modulus tensor.

For ideal elastoplastic material, the stress–strain behavior can be described as

$$\delta\varepsilon_{ij} = \frac{\delta S_{ij}}{2G} + \frac{\delta\sigma_m}{3K}\delta_{ij} + d\lambda\left(\frac{\partial F}{\partial\sigma_{kk}}\delta_{ij} + \frac{\partial F}{\partial S_{ij}}\right) \tag{8}$$

where K and G are the bulk and shear modulus of soils, which can be expressed by Young's modulus E and Poisson's ratio v as $K = \frac{E}{3(1-v)}$ and $G = \frac{E}{2(1+v)}$; σ_m and S_{ij} are the first invariant of principle stress and deviatoric stress tensor, respectively.

The Drucker–Prager yield criterion is used to describe the stress–strain behavior of thawing soil

$$\alpha_1\sigma_m + \sqrt{J_2} = k_1 \tag{9}$$

where J_2 are the second invariant of deviatoric stress, respectively.

The parameters α_1 and k_1 are defined as

$$\alpha_1 = \frac{2\sin\varphi}{\sqrt{3}(3-\sin\varphi)}, \quad k_1 = \frac{6c\cos\varphi}{\sqrt{3}(3-\sin\varphi)} \tag{10}$$

where c and φ are the cohesion and the angle of the internal friction.

A modified Richards' equation for freezing soil can be written as (Watanabe and Wake 2008)

$$\frac{\partial W_w}{\partial t} = \frac{\partial}{\partial z}\left(k(h)\frac{\partial h}{\partial z} + k(h) + k(h)\gamma h\frac{\partial T}{\partial z}\right) \tag{11}$$

where W_{w} is the equivalent liquid water content; z is a spatial coordinate; γ is the surface tension of soil water; h is the water pressure head, which can be obtained from the water retention curve in unfrozen domain while in frozen area, a simplified Clausius–Clapeyron equation was deduced as (Hansson et al. 2004)

$$\frac{dP}{dT} = \frac{L_f}{v_w T} \tag{12}$$

where P is the pressure ($P = \rho_{\mathrm{w}} g h$); L_{f} is the latent heat during freezing; v_{l} is the specific volume of water.

The equivalent water content W_{w} can be deduced as

$$W_w = W_u + \frac{\rho_i}{\rho_w} W_i \tag{13}$$

with an empirical relationship (Ma and Wang 2014)

$$W_u = a_1|T|^{-b_1} \tag{14}$$

where a_1 and b_1 are the experimental coefficients.

2.3 Rheological Element Based Creep Model for Frozen Soils

Following the work by Wang et al. (2014), the creep model based on the combination of some typical rheological element is given as (Wang et al. 2014)

$$\varepsilon_{ij} = \frac{\sigma_{ij}}{E_M} + \frac{\sigma_{ij}}{\eta_M}t + \frac{\sigma_{ij}}{E_K}\left[1 - \exp\left(-\frac{E_K}{\eta_K}t\right)\right], \quad \phi(F) \le 0 \tag{15a}$$

$$\varepsilon_{ij} = \frac{\sigma_{ij}}{E_M} + \frac{\sigma_{ij}}{\eta_M}t + \frac{\sigma_{ij}}{E_K}\left[1 - \exp\left(-\frac{E_K}{\eta_K}t\right)\right] + \frac{1}{\eta_N}\langle\phi(F)\rangle\frac{\partial Q}{\partial\{\sigma\}}t, \quad \phi(F) > 0 \tag{15b}$$

where E_{M} and E_{K} are the elastic modulus for Maxwell and Kelvin bodies, respectively; η_{M}, η_{K} and η_{N} are the coefficients of viscosity for Maxwell body, Kelvin body and Bingham body; and Q is a viscoplastic potential function. $\phi(F)$ is scaling function representing the magnitude of creep stage

$$\phi(F) = \left\langle \frac{F}{F_0} \right\rangle \tag{16}$$

where F_0 is the reference value, equal to 1.0 MPa for frozen soils.

A parabolic yield criterion suggest by Fish (1991) is defined as

$$F = \sqrt{3J_2} - c(T) - \sigma_m \tan\varphi(T) + \frac{\tan\varphi(T)}{2p_m}\sigma_m^2 \tag{17}$$

where p_m is the mean normal stress corresponding to the maximum shear stress q_m. For simplicity, the associated flow rule is employed here, i.e., $Q(\sigma_{ij})$ has the same form of the yield function $F(\sigma_{ij})$.

3 Computational Procedure

3.1 Key Technical Problems

During cyclic freeze and thaw processes, thaw consolidation and creep occurred in corresponding domains which varies with thermal state in frozen ground. The first key technical problem is to obtain a reliable thermal regime. This can be conveniently implemented in numerical analysis by using temperature dependent thermal indexes such as coefficient of heat conductivity and specific heat. The second is live calculation of thaw consolidation and creep in corresponding domains which is generally determined by the live thermal regime, i.e., thaw consolidation only occurred in domains at temperatures higher than soil freezing point when the drainage path is not blocked while creep initiated in other cases. The previous work by Wang et al. (2013) has provided a feasible way to solve this by embedding a section of code for judgment in the Fish language on the FLAC platform. The third is to synchronize the hydraulic and thermal calculations due to the fact that the hydraulic and thermal calculations were controlled by the corresponding timesteps, respectively, i.e., *fluid*dt and *th*dt (Itasca 1999). Yao et al. (2012) suggest a method by trial test and found that in the analysis of thaw consolidation, *fluid*dt $<$ *th*dt, timesteps are selected as *th*dt $= N_1$·*fluid*dt, where N_1 is an integer.

Moreover, there is still a challenge to be fulfilled, i.e., how to obtain the proportion of each source to the total settlement. From the monitored data of Qinghai–Tibet highway, we found that during the periodical freezing and thawing, frozen ground tends to thaw downward from the ground surface in the beginning of the warm season while for frozen soils underneath the thawing process is relatively later, during which the thaw settlement occurred under external load and gravity with the thawed water discharged. This process will last until the ground surface is frozen. Based on the phenomena above, Qi et al. (2012) defined a new conception of effective thaw consolidation time t_{eff}, as shown in Fig. 1. Note that creep of underlying permafrost layer also occurred in this phase. Except for this time, the drainage path is blocked and consolidation of thawing soils develops relatively slow; in the meantime, creep of underlying frozen and thawed soils dominates this period. The proportion of thaw consolidation and creep to the total settlement can be estimated from the following Fig. 2.

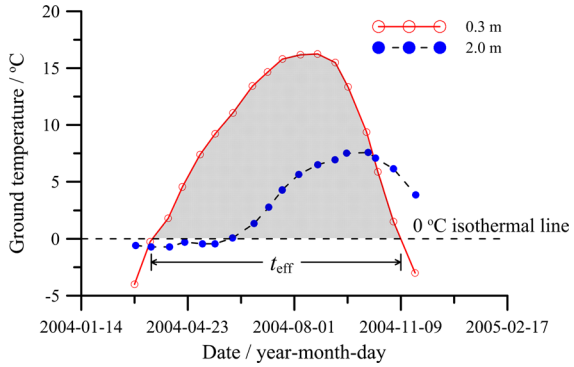

Fig. 1 Effective thaw consolidation time

3.2 Computational Procedure

Before analyzing settlement of embankment, the theoretical models presented in Sect. 2 are numerically implemented in the built-in Fish language on the FLAC platform. The computational procedures shown in Fig. 3 are as follows

Step I: The equivalent thermal indexes are assigned in the whole domain based on the initial temperature distribution such as $C(T)$ and $\lambda(T)$. Set the hydraulic and mechanical calculations off and only thermal mode is turned on, with duration of t_{ther};

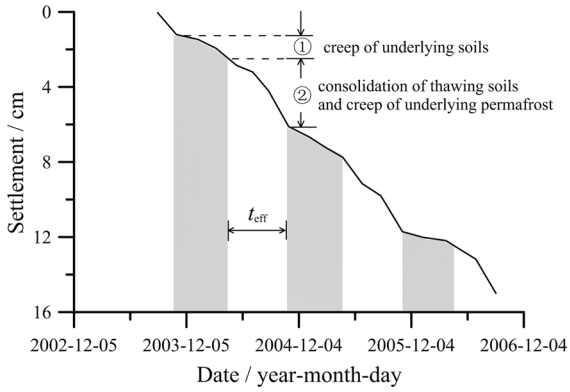

Fig. 2 The proportion of thaw consolidation and creep to total settlement

Step II: Call the newly compiled code to judge whether drainage paths are blocked or not, i.e., the temperature for elements in ground surface and slopes of embankment; in the meantime, the temperatures for elements will also be determined;

Step III: If drainage paths are blocked, i.e., $T(i,j) < 0$ °C, the creep model for soils will be assigned with the rheological parameters adjusted with temperature of elements; otherwise, the models for consolidation of thawing soils will be specified. Then set the thermal computation off and turn on the hydraulic and mechanical modes in thawed domain with duration of t_{con} equal to t_{ther} while for frozen area the thermal and hydraulic modes are set off and only the mechanical is carried out with duration of $t_{creep} = t_{ther} = N_{creep}*\Delta t_{creep}$, where N_{creep} is steps for creep analysis with Δt_{creep} as the corresponding timestep;

Step IV: Develop two arrays A(i,j) and B(i,j) to record the magnitude of thaw consolidation as well as the magnitude of creep of elements and give a live proportion of each source to total settlement;

Fig. 3 Computational procedure

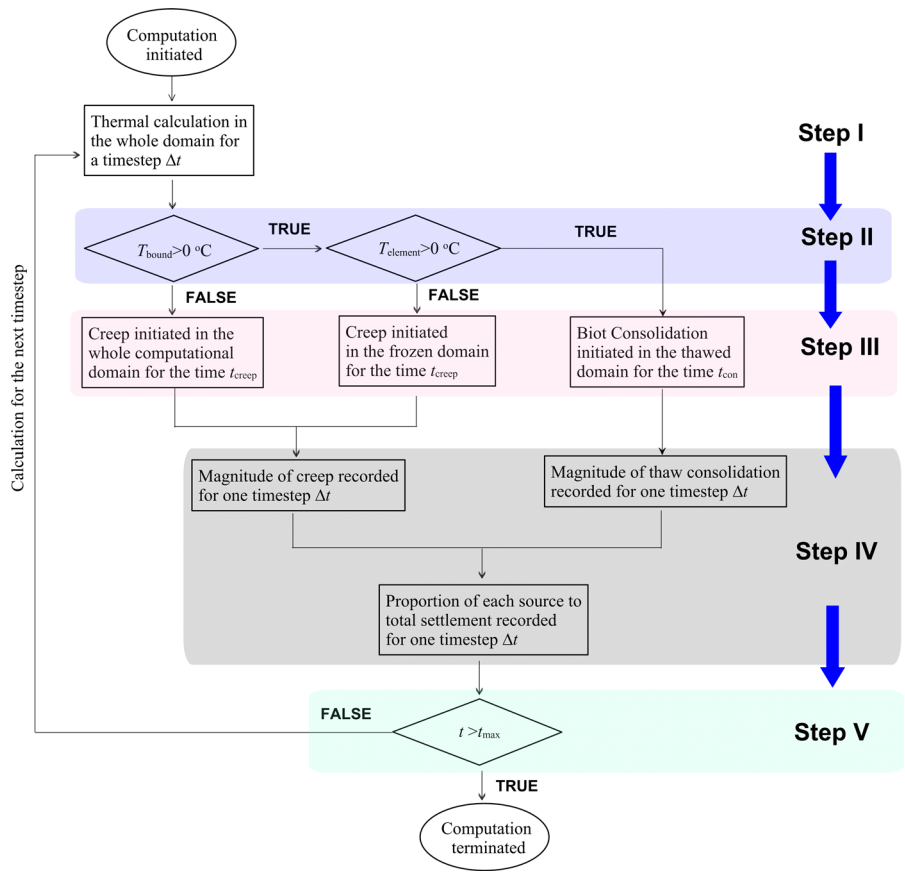

Step V: Set off hydraulic and mechanical modes and the whole computational domain will be reassigned by thermal indexes by the newly calculated thermal regime

The cycle from step (1) to (5) will stop when the target time is achieved.

4 Analysis of Settlement of Embankment

Two typical geological sections along the Qinghai–Tibet highway were taken as study object. The geological conditions were obtained from temperature monitoring boreholes, both of which include gravel, silty clay and well weathered mudstone. The specific location of each layer for two sections were illustrated in Fig. 4. The section H lies in the area at high ground temperature with a thick soil layer with ice inclusion while the section L is located at low temperature area with ice-rich permafrost layer.

In this study we assumed that the height of embankment for the two sections are 0, 1, 2, 3, 4, 5, and 6 m, with the width of pavement of 7.5 m and the grade of side slope of 1:1.5.

4.1 Boundary and Initial Conditions

Figure 5 presents the monitored temperatures of ground surface close to the two sections. We can observe that the temperatures for center of pavement, slope and natural ground surface all show a sinusoidal variation with time, which can be empirically estimated by the following equation

$$T = T_0 + \alpha t + A \sin\left(\frac{2\pi t}{365} + n\pi\right) \tag{18}$$

where, T_0 is the mean annual temperature; A is the amplitude of temperature; $n\pi$ is the initial phase; α is the annual warming rate. Considering the potential

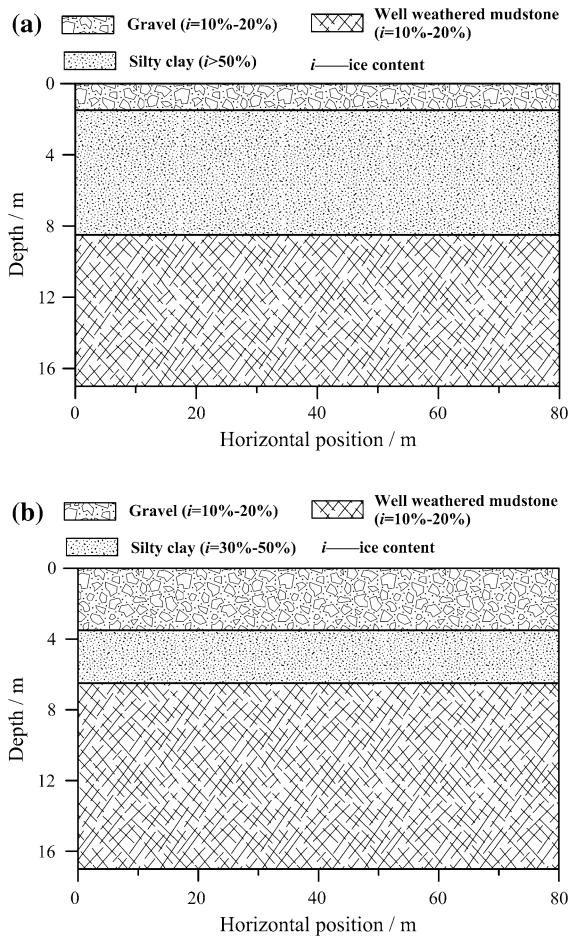

Fig. 4 **a** Geological conditions, H section. **b** Geological conditions, L section

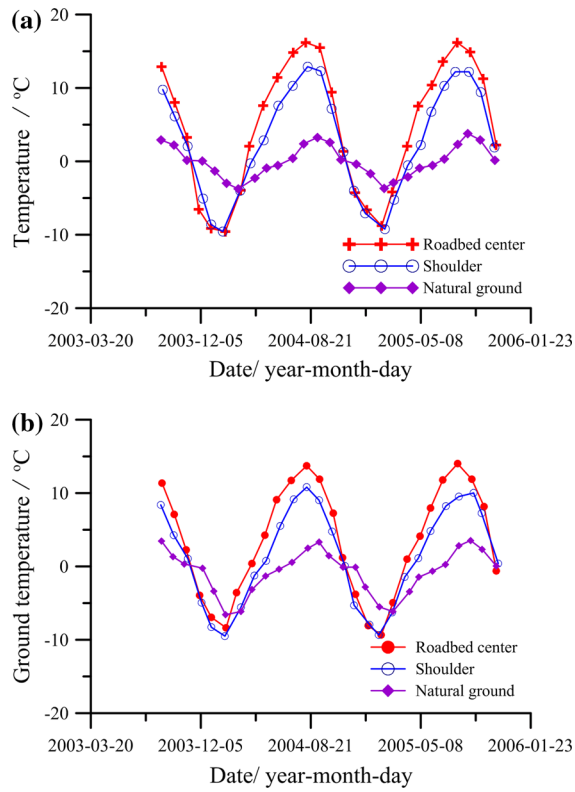

Fig. 5 **a** Monitored temperatures, H section. **b** Monitored temperatures, L section

effect of global warming, the annual mean temperature for the Qinghai–Tibetan plateau will increase by 2.6 °C in the following 50 years (Qin 2002). The parameters for thermal boundaries can be fitted from the monitored data, as listed in Table 1.

The monitored temperature data on Sept. 2003 in the natural borehole was taken as the initial thermal state for numerical computation, as shown in Fig. 6. The permafrost table h_{nat} for two monitored sections are 1.40 and 1.90 m, respectively. For sake of safety, the initial temperature for the fill of embankment is taken to be 10 °C and the heat flux on the bottom boundary of the numerical model is 0.02 °C/m. Both sides of the model is assumed to be adiabatic.

The additional settlement of embankment induced by vehicular load is significant and is generally simplified as a uniformly distributed static load on roadbed pavement based on highway capacity (Lai et al. 2009). Here, we assumed the uniform load on the pavement of the Qinghai–Tibet highway to be 11.5 kPa (Wang et al. 2013). As for the mechanical boundaries, the free displacement boundary include roadbed pavement, shoulder and natural ground. Both sides of the computational model is assumed to be displacement free in x direction, with a y-direction displacement fixed on the bottom. Due to the fact that the asphalt pavement is low-permeability material, we assumed that the pavement is impermeable and the free drainage boundaries are shoulder of embankment and natural ground.

4.2 Parameters for Thaw Consolidation and Creep

Based on the geological exploration and in situ tests, we obtained the physical parameters for two sections, as listed in Table 2. Considering the ice-water phase change of underlying geo-materials, the equivalent specific heat for soils in each layer is shown in Table 3.

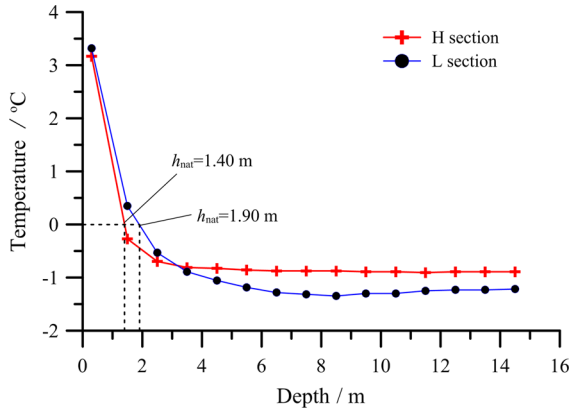

Fig. 6 Initial thermal state for numerical computation

For thaw consolidation of underlying permafrost, we should firstly specify the hydraulic conductivity for soils in frozen or thawed state. Here we followed the work by Watanabe and Flury (2008) and Engelmark (1984) and give the hydraulic conductivity for soils, as listed in Table 4. Moreover, the mechanical properties of soils at various temperatures can be estimated by a set of empirical equations (Li et al. 2009). Based on test results (Ma and Wang 2014), we obtained the mechanical properties such as elastic modulus, Poisson's ratio, cohesion and angle of internal friction, as listed in Table 5.

From previous experimental work (Bray 2013; Ma and Wang 2014), we found that for frozen soils at higher ice content, especially frozen soils with ice inclusion, the magnitude of creep may be more significant than those at lower ice content. Due to the actual stress state, creep of fill and gravel is not taken into account. Besides, compared with weathered mudstone, creep of frozen silty clay at ice contents higher than 30 % should be paid more attention. Table 6 presents the creep parameters for frozen silty clay at higher ice contents.

Table 1 Fitted parameters for thermal boundary

Section	Parameter	Roadbed center	Shoulder	Natural ground
H section	A	12.75	10.64	3.62
	T_0	3.33	2.04	−0.22
	n	1/2	1/2	1/3
L section	A	11.35	9.98	5.00
	T_0	2.42	0.20	−1.66
	n	1/2	1/2	1/3

Table 2 Physical parameters for underlying soils

Section	Geological condition	Dry unit weight (kN/m^3)	Water content (%)	Coefficient of heat conductivity (W/(m °C))	
				Frozen	Thawed
Fill	Fill	20.50	10	1.71	1.31
H section	Gravel	18.50	20	1.45	1.28
	Silty clay	16.40	40	1.45	0.86
	Well weathered mudstone	20.70	15	0.96	0.91
L section	Gravel	18.50	20	1.45	1.28
	Silty clay	21.20	19	1.38	1.24
	Well weathered mudstone	20.70	15	0.96	0.91

Table 3 Equivalent specific heat for underlying soils (J/kg °C)

Section	Geological condition	Soil temperature (°C)								
		20.0–0.0	0.0 to −0.2	−0.2 to −0.5	−0.5 to −1.0	−1.0 to −2.0	−2.0 to −3.0	−3.0 to −5.0	−5.0 to −10.0	−10.0 to −20.0
Fill	Fill	2183	72,405	11,060	4497	3156	2004	1973	1820	1693
H section	Gravel	2484	91,594	18,245	8631	3737	2799	2367	2032	1844
	Silty clay	1794	130,278	35,903	11,864	6678	6640	2702	1737	1283
	Well weathered mudstone	2191	2267	29,562	15,080	5160	3958	2564	2076	1907
L section	Gravel	2484	91,594	18,245	8631	3737	2799	2367	2032	1844
	Silty clay	1397	103,562	29,635	9842	5268	4640	2400	1549	1149
	Well weathered mudstone	2191	2267	29,562	15,080	5160	3958	2564	2076	1907

Table 4 Hydraulic conductivity for underlying soils

Section	Geological condition	k (m/s)	
		Thawed	Frozen
Fill	Fill	1.0×10^{-7}	1.0×10^{-19}
H section	Silty clay	1.3×10^{-7}	1.3×10^{-19}
	Well weathered mudstone	2.3×10^{-8}	2.3×10^{-20}
	Gravel	5.0×10^{-9}	5.0×10^{-21}
L section	Silty clay	1.3×10^{-7}	1.3×10^{-19}
	Well weathered mudstone	1.4×10^{-8}	1.4×10^{-20}
	Silty clay	5.0×10^{-9}	5.0×10^{-21}

4.3 Discussion on the Reasonable Height of Embankment

For highway engineering in cold regions with low embankment, a continuing warming in the underlying permafrost occurs due to the weak heat resistance of subgrade body, which facilitates the settlement of embankment. For higher embankments, the permafrost table may ascend upward and into the subgrade body when a new thermal balance is formed

Table 5 Mechanical properties of underlying soils

Section	Geological condition	Mechanical properties	Soil temperature (°C)							
			−20	−10	−5	−2	−1	−0.05	0	20
Fill	Fill	E (MPa)	31.2	28	25	23	22	21.2	21	21
		v	0.13	0.13	0.13	0.14	0.19	0.22	0.24	0.24
		c (MPa)	0.8	0.7	0.5	0.3	0.1	0.03	0.001	0.001
		φ (°)	40	40	40	40	40	38	28	28
H section	Gravel	E (MPa)	72.6	61.3	50.8	45	40	36.9	34	34
		v	0.13	0.13	0.13	0.14	0.19	0.35	0.45	0.45
		c (MPa)	0.6	0.6	0.6	0.6	0.6	0.15	0.003	0.003
		φ (°)	34	34	34	34	34	31	30	30
	Silty clay	E (MPa)	262.5	127.5	66	27.7	4.9	1.1	0.75	0.75
		v	0.15	0.15	0.18	0.2	0.22	0.24	0.4	0.4
		c (MPa)	1.3	1.3	1.3	1.3	1.3	0.1	0.007	0.007
		φ (°)	25	25	25	22	14	12	12	12
	Well weathered mudstone	E (MPa)	880	790	731	666	572	500	500	500
		v	0.25	0.25	0.25	0.25	0.25	0.25	0.25	0.25
		c (MPa)	38	38	38	38	38	38	32	32
		φ (°)	28	28	28	28	28	28	14	14
L section	Gravel	E (MPa)	72.6	61.3	50.8	45	40	36.9	34	34
		v	0.13	0.13	0.13	0.14	0.19	0.35	0.45	0.45
		c (MPa)	0.6	0.6	0.6	0.6	0.6	0.15	0.003	0.003
		φ (°)	34	34	34	34	34	31	30	30
	Silty clay	E (MPa)	1050	510	264	111	19.8	4.5	3	3
		v	0.15	0.15	0.18	0.2	0.22	0.24	0.4	0.4
		c (MPa)	3.9	3.9	3.9	3.9	3.9	0.3	0.03	0.03
		φ (°)	25	25	25	22	14	12	12	12
	Well weathered mudstone	E (MPa)	880	190	731	666	572	500	500	500
		v	0.25	0.25	0.25	0.25	0.25	0.25	0.25	0.25
		c (MPa)	38	38	38	38	38	38	32	32
		φ (°)	28	28	28	28	28	28	14	14

Table 6 Creep parameters for underlying soils

Section	T (°C)	E_M (MPa)	E_K (MPa)	η_M (MPa h)	η_K (MPa h)	η_N (MPa h)
H section	−20	111.44	162.18	142.39	23.33	2996.86
	−5	59.66	41.12	7380	251.53	154.08
	−1	45.53	13.21	17,758	562.05	74.53
	0	43.13	3.11	28,135	660.10	58.62
	20	42.56	2.05	158,728	687.18	54.65
L section	−20	328.85	524.08	74.46	605.91	687.98
	−5	119.30	76.83	7117.32	74.53	106.78
	−2	97.40	52.33	17,717.12	49.02	73.56
	0	85.08	40.51	32,542.00	37.07	57.38
	20	68.85	34.09	43,516.00	30.60	48.80

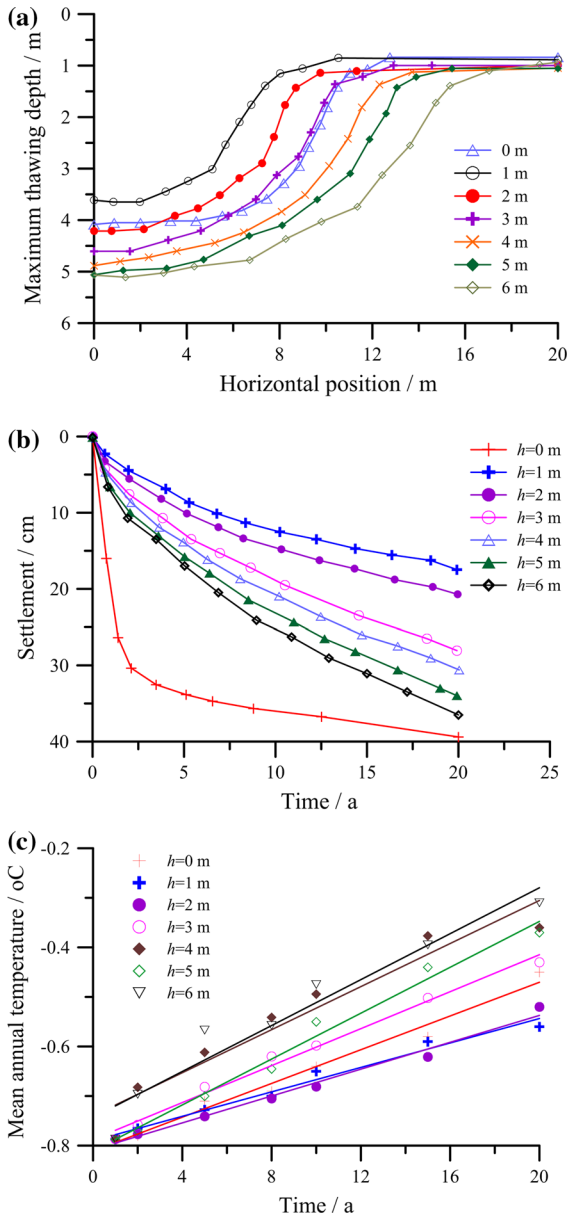

Fig. 7 **a** Temperature and settlement for embankments, maximum thawing depth. **b** Temperature and settlement for embankments, mean annual temperature. **c** Temperature and settlement for embankments, settlement in roadbed center

with the original ground temperature recovered (Lai et al. 2009). However, due to the higher ground pressure in high embankments, creep may develop continuously, especially for warm and ice-rich permafrost area (Qi et al. 2007). Thus, a reasonable height of embankment for highways in cold regions is particularly important for operating and maintenance.

Here, we select the section at higher ground temperature, i.e., H section, to analyze the range for the reasonable height of embankment based on thermal and mechanical responses. Figure 7 illustrates the maximum thawing depth, mean annual temperature of silty clay and settlement in the roadbed center for embankments at various heights.

From the above figure, we can see that as the height of embankment increases, the maximum thawing depth, the mean annual temperature in silty clay and settlement in the roadbed center all show complex changes. For better illustrating the effect of height of embankment on thermal and mechanical responses, we select the numerical data in 20 years to analyze the reasonable height of embankment, as presented in Fig. 8. It shows that as the height of embankment increases, maximum thawing depth, mean annual temperature in silty clay and settlement in roadbed center manifest similar tendency that at a height of 1.0–2.0 m, the aforementioned three indexes tends to minimize, which indicates a relatively reasonable height of embankment.

To verify the rationality of numerical results, the critical and design height of embankment for the Qinghai–Tibet highway is proposed based on ice content in permafrost table and filled soil type (Wu and Liu 2005), as shown in Table 7. Moreover, an empirical equation was proposed to estimate the minimum height of fill under asphalt pavement (Wu and Liu 2005).

$$H_0 = 2.40 - 0.55 \cdot h_{nat} \tag{19}$$

where H_0 is the critical height of embankment under asphalt pavement; h_{nat} is the permafrost table.

The critical height of embankment for section H can be calculated by substituting the permafrost table in Fig. 6 into Eq. (19), equal to 1.63 m, which lies within the range of 1.0–2.0 m. The design height for section H is 1.96–2.12 m correspondingly. For sake of convenience, the design height for H section is taken to be 2.0 m. Besides, by utilizing the same method, the critical and design heights for section L are 1.35 and 1.60 m, respectively.

4.4 Development of Thawing Depth and Settlement

According to the design height of embankment for two sections, we calculate the development of thawing

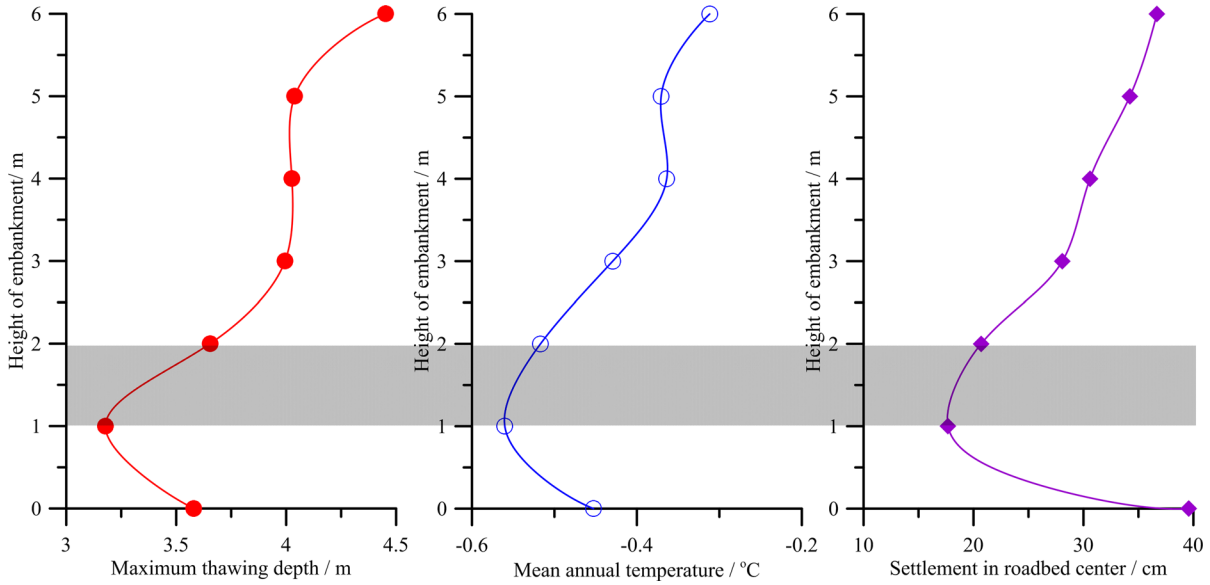

Fig. 8 Comparison of thermal and mechanical responses of embankment at various heights

Table 7 Critical and design height for embankment with asphalt pavement

Ice content (%)	Permafrost table (m)	Critical height (m)	Design height (m)
10–20	>2.5	<1.03	$0.6–0.7H_0$
20–30	2.0–2.5	1.03–1.30	H_0
30–50	1.6–2.0	1.30–1.52	$1.1–1.2H_0$
>50	1.2–1.8	1.40–1.74	$1.2–1.3H_0$

depth and settlement in 20 years. Figure 9 illustrates the development of thawing depth for two sections. It indicates that for two sections the maximum thawing depth develops downward with time and due to heat absorption of asphalt pavement the permafrost table under roadbed center develops faster than that under shoulder of embankment as well as natural surface. Moreover, we also observe a faster development of permafrost table in section H due to more intense ice-water phase change in silty clay with ice inclusion. This also reveals that the continuing thawing processes occurs beneath two sections and settlement may be significant in two key positions, i.e., shoulder of embankment and asphalt pavement.

We can notice from Fig. 10 that settlement of embankment for two sections also increases with time and larger deformation is observed in the aforementioned two key positions, i.e., shoulder of embankment and asphalt pavement. Also, we can see a larger deformation in section H, which is closely related to the higher magnitude of thaw consolidation induced by faster development of maximum thawing depth; besides, the continuous warming in underlying permafrost will lead to larger creep deformation as well.

4.5 Proportion of Thaw Consolidation and Creep in Total Settlement

Figure 11 shows the development of thaw consolidation in each layer including fill, gravel and silty clay. We can notice that due to the higher degree of compaction and lower ice content, the deformation of fill is relatively small for two sections. For gravel

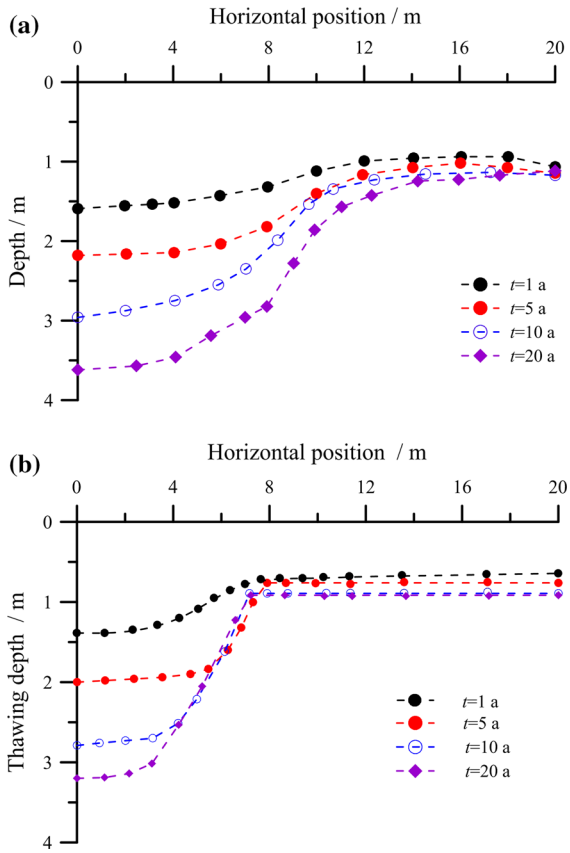

Fig. 9 **a** Development of maximum thawing depth, H section. **b** Development of maximum thawing depth, L section

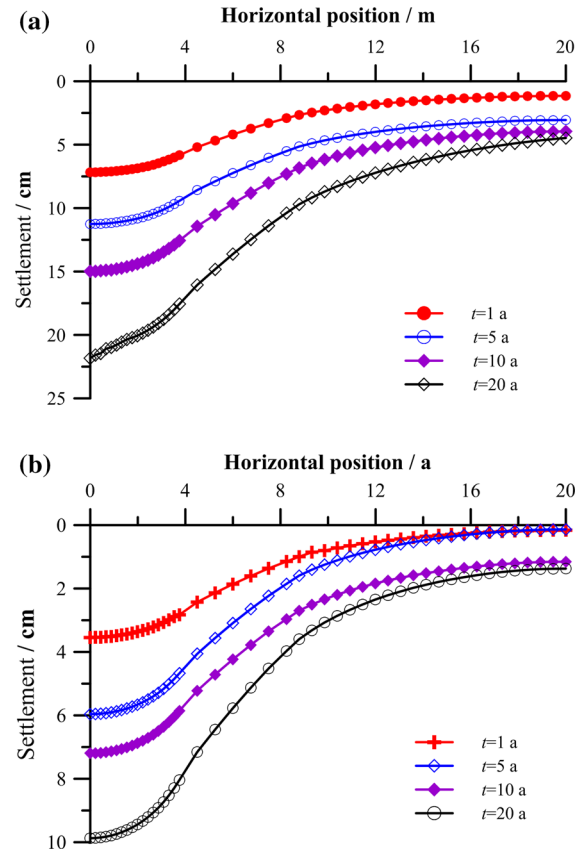

Fig. 10 **a** Settlement of embankment, H section. **b** Settlement of embankment, L section

layer, thaw consolidation will quickly finish due to the coarse grain and short drainage path and the magnitude of thaw consolidation is relatively small. As for the silty clay, thaw consolidation strongly depends on both the development of maximum thawing depth and ice content, manifesting as larger thaw consolidation in H section than that in L section. In addition, the higher temperature in silty clay layer and more ice inclusion also cause larger creep in section H, as presented in Fig. 12.

Figure 13 illustrates the comparison of thaw consolidation and creep for two sections. Here for sake of simplicity, we use TC and Cr to represent the deformation induced by thaw consolidation and creep, respectively. It indicates that for section H, the maximum thawing depth has developed into the silty clay layer with ice inclusion in 1 year of operation and thaw consolidation account for a major part in the total settlement within the computation duration while creep of warm frozen soils is also significant, approximately 5.8 cm in 20 years. Moreover, for section L, the maximum thawing depth has not reached the ice-rich silty clay layer. Thus, thaw consolidation only occurs in the fill and gravel layers but due to the coarse grained structure of gravel and low ground pressure in fill, thaw consolidation occupies 50 % of the total settlement while creep of underlying warm frozen soils also results in an obvious time-dependent settlement. The differences for sections H and L in the proportions of thaw consolidation and creep to the total settlement may be related to thermal boundaries as well as the depth of frozen soils at higher ice contents or with ice inclusion.

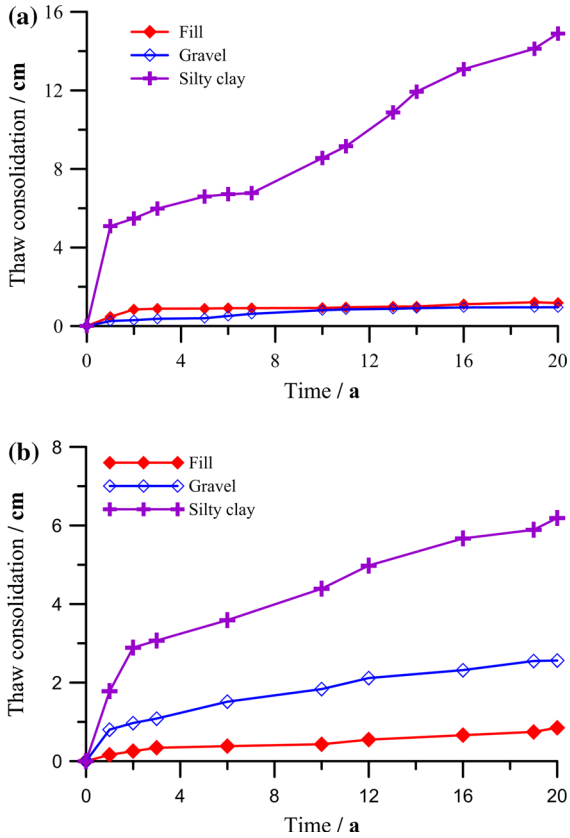

Fig. 11 **a** Thaw consolidation of each layer under roadbed center, H section. **b** Thaw consolidation of each layer under roadbed center, L section

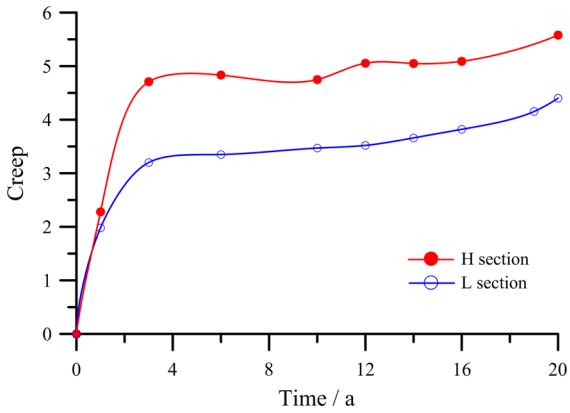

Fig. 12 Creep of silty clay under roadbed center

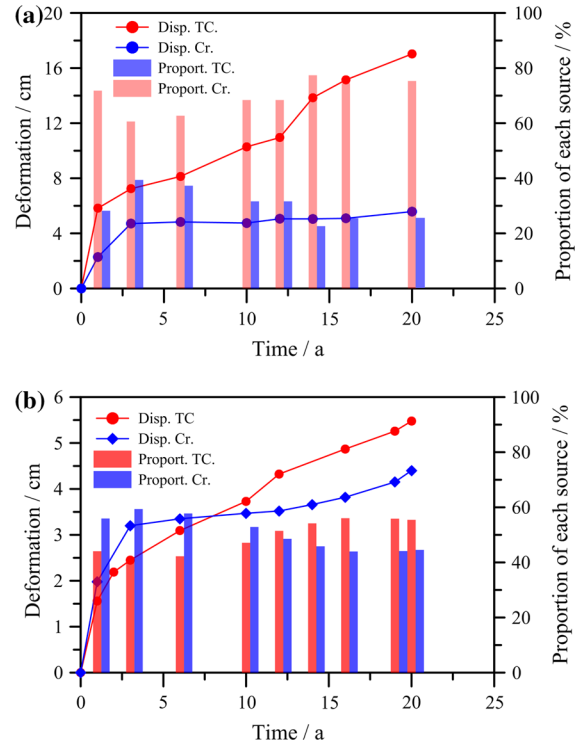

Fig. 13 **a** Proportion of thaw consolidation and creep, H section. **b** Proportion of thaw consolidation and creep, L section

5 Conclusions

This paper presents a numerical study on the reasonable height of embankment for highway engineering in cold regions. An improved method for estimating settlement of foundations in cold regions were put forward by embedding a section of code by post-processing the settlement induced by various sources of settlement.

Two typical geological sections were selected along the Qinghai–Tibet highway and at assumed depth of embankment as 0–6 m, maximum thawing depth, mean annual temperature in permafrost layer at higher ice contents, as well as settlement in the roadbed center in 20 years of operation were compared, which further indicates a reasonable height of 1.63 and 1.35 m for sections H and L, respectively.

Based on the conception of effective thaw consolidation time, the proportions of thaw consolidation and creep to the total settlement were analyzed. Results show that after 20 years of operation thaw consolidation accounts for a major part in total settlement for section H at higher ground temperature and creep also occupies a significant proportion. For section L at lower ground temperature, the proportion of thaw consolidation is a little larger than that of creep.

Acknowledgments This research was financially supported in part by the National Natural Science Foundation of China (Nos. 51408486 and 41172253). These supports are greatly appreciated.

References

Andersland OB, Ladanyi B (1994) An introduction to frozen ground engineering. Chapman and Hall, New York

Bray MT (2013) Secondary creep approximation of ice-rich soils and ice using transient relaxation tests. Cold Reg Sci Technol 88:17–36

Engelmark H (1984) Infiltration in unsaturated frozen soil. Nord Hydrol 15:243–252

Epps A (2000) Design and analysis system for thermal cracking in asphalt concrete. J Transp. Eng. 126(4):300–307

Fish AM (1991) Strength of frozen soil under a combined stress state. In: Proceedings of 6th international symposium on ground freezing, pp 135-145

Hansson K, Šimůnek J, Mizoguchi M, Lundin LC, van Genuchten MT (2004) Water flow and heat transport in frozen soil: numerical solution and freeze-thaw application. Vadose Zone J 3:693–704

Heike L, Peter A (2000) Global warming: a climate of uncertainty. Nature 408:896–897

Itasca (1999) Flac manual: theoretical background. Itasca Consulting Group, Minneapolis

Ladanyi B (1972) An engineering theory of creep of frozen soil. Can Geotech J 22(9):88–99

Lai Y, Zhang M (2003) Cooling effect of ripped-stone embankments on Qinghai–Tibet railway under climatic warming. Chin Sci Bull 48(6):598–604

Lai Y, Zhang M, Li S (2009) Theory and application of cold regions engineering. Science Press, Beijing **(in Chinese)**

Li S, Lai Y, Zhang M, Yuanhong Dong (2009) Study on the long-term stability of Qinghai–Tibetan railway embankment. Cold Reg Sci Technol 57:139–147

Ma W, Wang D (2014) Mechanics of frozen ground. Science Press, Beijing **(in Chinese)**

Ma W, Fang L, Qi J (2011) Methodology of study on freeze-thaw cycling induced changes in engineering properties of soils. In: Proceedings of the 9th international symposium on permafrost engineering, vol 9. pp 38–43

Morgenstern NR, Nixon JF (1971) One-dimensional consolidation of thawing soils. Can Geotech J 8(4):558–565

Qi J, Yu S, Zhang J, Wen Z (2007) Settlement of embankments in permafrost regions in the Qinghai–Tibet Plateau. Nor J Geogr 61(2):49–55

Qi J, Yao X, Yu F, Liu Y (2012) Study on thaw consolidation of permafrost under roadway embankment. Cold Reg Sci Technol 81:48–54

Qin DH (2002) Assessment on environment of western China. Science Press, Beijing **(in Chinese)**

Thomas RK, Kevin ET (2003) Modern global climate change. Science 302:1719–1723

Tong C, Wu Q (1996) The effect of climate warming on Qinghai–Tibet highway, China. Cold Reg Sci Technol 24(1):101–106

Vyalov CC (1986) Rheological fundamentals of soil mechanics. Elsevier, New York

Wang S, Liu F (2015) A hypoplasticity-based method for estimating thaw consolidation of frozen sand. Geotech Geol Eng. doi:10.1007/s10706-015-9902-8

Wang S, Qi J, Yu F, Yao X (2013) A novel method for estimating settlement of embankment in cold regions. Cold Reg Sci Technol 88:50–58

Wang S, Qi J, Yin Z, Zhang J, Ma W (2014) A simple rheological element based creep model for frozen soils. Cold Reg Sci Technol 106–107:47–54

Watanabe K, Flury M (2008) Capillary bundle model of hydraulic conductivity for frozen soil. Water Resour Res 44:W12402

Watanabe K, Wake T (2008) Hydraulic conductivity of frozen unsaturated soil. In: Proceedings of 9th international conference permafrost, pp 147–152

Wu Z, Liu Y (2005) Frozen ground and engineering construction. China Ocean Press, Beijing **(in Chinese)**

Wu Z, Zhu L, Guo X, Wang X, Fang J (1998) Critical height of the embankment in the permafrost regions along the Qinghai–Kangding highway. J Glaciol Geocryol 20(1):36–41 **(in Chinese)**

Wu Q, Li X, Li W (2001) The response model of permafrost along the Qinghai–Tibetan highway under climate change. J Glaciol Geocryol 23(1):1–5 **(in Chinese)**

Wu Q, Liu Y, Zhang J, Tong C (2002) A review of recent frozen soil engineering in permafrost regions along Qinghai–Tibet highway, China. Permafrost Periglac Process 13(3):199–205

Yao X, Qi J, Wei Wu (2012) Three dimensional analysis of large strain thaw consolidation in permafrost. Acta Geotech 7:192–202

Yu W, Wu J (1986) The problem of embankment height under asphalt pavement in permafrost regions on Qinghai–Xizang highway. Professional Papers of Highway Engineering Studies on Permafrost of Qinghai–Xizang Plateau. Xi' an: Xi' an Institute of Highway, pp 25–47. (in Chinese)